

1 Calibrating the exchange coefficient in the modified  
2 coupled continuum pipe-flow model for flows in  
3 karst aquifers

4 Nan Chen<sup>a</sup>, Max Gunzburger<sup>b</sup>, Bill Hu<sup>c</sup>, Xiaoming Wang<sup>d,\*</sup>,  
Celestine Woodruff<sup>e</sup>

<sup>a</sup>*School of Mathematical Sciences, Fudan University, Shanghai, China, 200433.*  
*Email: chennan@fudan.edu.cn.*

<sup>b</sup>*Department of Scientific Computing, Florida State University, Tallahassee, FL,*  
*32306-4120. Email: gunzburg@fsu.edu.*

<sup>c</sup>*Department of Earth, Ocean and Atmospheric Science, Florida State University,*  
*Tallahassee, FL, 32306-4520. Email: hu@gly.fsu.edu.*

<sup>d</sup>*Department of Mathematics, Florida State University, Tallahassee, FL, 32306-4510.*  
*Email: wxm@math.fsu.edu.*

<sup>e</sup>*Department of Mathematics, Florida State University, Tallahassee, FL, 32306-4510.*  
*Email: cwoodruf@mail.math.fsu.edu.*

5 **Abstract**

6 We investigate the validity of the popular coupled-continuum pipe-flow  
7 (CCPF) model for flow in a karst aquifer. The (Navier) Stokes-Darcy model  
8 is used as the “true model” for calibrating the exchange coefficient in the  
9 CCPF model by minimizing the relative differences between results from the  
10 two models or at least by having those differences being below a prescribed  
11 threshold value. We find that although the CCPF model is never in perfect  
12 agreement with the Stokes-Darcy model, there is an almost universal choice for  
13 a nearly optimal exchange coefficient such that the relative error is below one  
14 percent. Our numerics suggest that the nearly optimal choice of the exchange  
15 coefficient should be sufficiently large instead of being a small quantity that is

---

\*Corresponding author. Email Address: wxm@math.fsu.edu. Address: 208 James J. Love Building, Department of Mathematics, Florida State University, 1017 Academic Way, Tallahassee, FL, 32306-4510, USA. Tel.: +1 850 644 6419; Fax.: +1 850 644 4053.

16 proportional to the hydraulic conductivity, as suggested in existing literatures.  
17 We also show that this nearly optimal choice of exchange coefficient is robust  
18 under a wide range of model parameters. This result demonstrates that the  
19 CCPF model is a valid approximation for flows in karst aquifers as long as we  
20 set the fluid exchange coefficient sufficiently large and at least in the simple  
21 two-dimensional setting that we consider.

22 *Key words:* exchange coefficient, coupled-continuum pipe-flow (CCPF) model,  
23 Stokes-Darcy model, karst aquifer

## 24 **1 Introduction**

25 Well developed karst aquifers, in addition to a porous limestone matrix, typically  
26 have large cavernous conduits that are known to largely control groundwater flow  
27 and contaminant transport within the aquifer (Katz et al. 1998). One of the com-  
28 monly used approaches to fluid flow in karst aquifers is the coupled continuum  
29 pipe-flow model (CCPF) (Bauer et al. 2000, 2003; Birk et al. 2003; Chen et al.  
30 1988; Kiral 1998; MacQuarrie et al. 1996). The CCPF model is a dual flow sys-  
31 tem consisting of a matrix representing the bulk mass of permeable limestone and a  
32 conduit system representing the karst conduit network. Flow exchange between the  
33 two systems is controlled by differences in hydraulic heads as well as the hydraulic  
34 conductivity and the geometric setting. In the CCPF model, the groundwater flow  
35 in the matrix is described by the Darcy’s law and the flow in the conduit is modeled  
36 by a pipe-flow model. The water mass exchange flow rate between the two systems is  
37 described by a first-order mass exchange model; the exchange flow rate is assumed to  
38 be linearly proportional to the head difference between the two systems (Barenblatt  
39 et al. 1960; Sauter 1992; Teutsch 1989). The exchange rate coefficient, denoted  $\alpha_{ex}$ ,  
40 is a crucial parameter. It is a lumped parameter and its value will depend on many  
41 factors including, among others, the hydraulic conductivity in the matrix, the ex-

42 change surface between the conduit and matrix, and conduit geometry (Barenblatt  
43 et al. 1960; Liedl et al. 2003). The value of the exchange rate parameter is not  
44 usually obtained from measurements but rather through curve-fitting. This CCPF  
45 model was utilized in studying conduit genesis (Bauer et al. 2000; 2003; Birk et al.  
46 2003; Clemens et al. 1996; Liedl et al. 2003) and is now incorporated in the latest  
47 version of the US Geological Survey’s popular groundwater software MODFLOW (  
48 Shoemaker et al. 2008; Harbaugh 2005) (The conduit flow process part is usually  
49 termed CFP).

50 A major advantage of this approach is its relative simplicity and computational  
51 efficiency compared to other models (i.e. the coupled Stokes-Darcy system). Ex-  
52 isting literature suggests that  $\alpha_{ex}$  should be set to the order of the hydraulic con-  
53 ductivity (Bauer et al. 2000, 2003). Even so, it has been observed that there is  
54 high sensitivity of the solution in this regime of the parameter (Bauer et al. 2000,  
55 2003; Birk et al. 2003; Hua 2009; Liedl et al. 2003). Therefore, there is an urgent  
56 need to provide guidance on the selection of this critical exchange parameter as  
57 well as the validity of the CCPF model. On the other hand, there is an alternative  
58 approach for laminar fluid flows in karst aquifers using the coupled Stokes (in the  
59 conduit) and Darcy (in the matrix) model (Cao et al. 2010; Discacciati et al. 2002;  
60 Faulkner et al. 2009, Layton et al. 2003). The two flow systems are coupled via  
61 the empirical Beavers-Joseph interface boundary condition and the model is known  
62 to be physically and mathematically sound (Beavers and Joseph 1967; Cao et al.  
63 2010b; Discacciati et al. 2002, Saffman 1971). It has been demonstrated that this  
64 model can capture the fluid flow and the transport of contaminants very well in a  
65 controlled environment (Faulkner et al. 2009). Therefore, it makes sense for us to  
66 assess the validity of CCPF model, assuming that the coupled Stokes-Darcy model  
67 is the “true model”.

68 In this work, we address the following **important issues**:

- 69 • What is the (near) optimal choice of the fluid exchange coefficient  $\alpha_{ex}$  so

70 that the relative error between the solution to the coupled continuum pipe-  
 71 flow model and the solution of the established coupled Stokes-Darcy model is  
 72 (essentially) minimized?

- 73 • How does the (near) optimal choice of exchange coefficient depend on the  
 74 system parameters?
- 75 • How does the minimum discrepancy (under the near optimal choice of exchange  
 76 coefficient) between the two models depend on the system parameters?

77 There are several natural criteria that can be used to measure the discrepancy  
 78 between the solutions of the two models. These different criteria will be discussed  
 79 in detail later in section 4.

80 The problem that we propose to tackle here is a difficult one since it is an  
 81 optimization problem constrained by partial differential equations (PDEs). In order  
 82 to make the problem relatively amenable, we will make the following **assumptions**:

- 83 1. We consider a conceptual two dimensional domain for a karst aquifer with a  
 84 straight horizontal conduit imbedded in the middle of a rectangular porous  
 85 media (or matrix). In the coupled continuum pipe-flow model (CCPF), the  
 86 conduit will be simplified to a line located at  $y = 0$ , *i.e.*,  $\Omega_c = (0, L) \times \{y = 0\}$ .  
 87 The matrix domain takes the form of  $\Omega_m = (0, L) \times (0, H_m) \cup (0, L) \times (-H_m, 0)$   
 88 where  $2H_m$  represents the height of the matrix,  $L$  is the horizontal length of the  
 89 conduit and matrix. In the case of Stokes-Darcy model, the conduit domain  
 90 is  $\Omega_c = (0, L) \times (-H_c, H_c)$ , and the matrix is  $\Omega_m = (0, L) \times (H_c, H_c + H_m) \cup$   
 91  $(0, L) \times (-H_m - H_c, -H_c)$
- 92 2. We will assume that the matrix is homogeneous and isotropic with constant  
 93 permeability  $\Pi$ , and hence constant hydraulic conductivity  $\mathbb{K} = \frac{\Pi g}{\nu}$ , where  
 94  $\nu$  is the kinematic viscosity of the fluid (water) and  $g$  is the gravitational  
 95 acceleration constant.

96 3. We investigate the laminar flow regime so that the relatively simple Stokes-  
97 Darcy model and the laminar CFP model are applicable.

98 4. We consider constant Neumann type boundary condition (equivalent to con-  
99 stant fixed flux) so that the laminar CCPF model and Stokes-Darcy model  
100 can be reduced to systems of ordinary differential equations in terms of the  
101 Fourier coefficients in the horizontal direction. (Of course Fourier expansion  
102 is not applicable in the original variable but can be used after an appropriate  
103 translation of the unknown.)

104 The linear constant coefficient ODE systems can be reduced to systems of linear  
105 algebraic equations in the setting that we have adopted here. The optimization (to  
106 minimize the difference between the CCPF model and the Stokes-Darcy model) is  
107 then performed on the reduced linear algebraic systems for parameter regime that  
108 corresponds to the Wakulla Spring in Florida (Tincaid 2004). Instead of only search-  
109 ing for the optimal exchange coefficient that absolutely minimizes the discrepancy  
110 between the two models, we also identify those values of exchange coefficient so that  
111 the relative error is less than or equal to one percent (1%). Such an approach is  
112 sensible especially in the presence of uncertainties in terms of geometry, hydraulic  
113 conductivity, boundary conditions etc. The (near) optimal fluid exchange coefficient  
114  $\alpha_{ex}$  depends on the criterion that we use as expected. However, the conventional  
115 choice of an order one constant multiply the hydraulic conductivity does not seem  
116 to work. Instead, our study suggests a universal near optimal choice of about 25 for  
117 the fluid exchange coefficient so that the relative error is below 1% no matter which  
118 matching criterion is used. Moreover, this near optimal choice of fluid exchange co-  
119 efficient is robust with respect to change of parameters up to an order of magnitude  
120 (low sensitivity). This gives us strong indication of the validity of the simplified  
121 CCPF model provided that we set the fluid exchange coefficient to the near optimal  
122 value (25 for instance).

123 The rest of the paper is organized as follows. We recall the CCPF model and

124 derive its solution formula in section 2. The coupled Stokes-Darcy model is then  
 125 investigated in Section 3. We calibrate the exchange coefficient in the CCPF model  
 126 by matching the solutions to the CCPF model and the Stokes-Darcy model numeri-  
 127 cally in Section 4 under various parameter setting and different matching criterions.  
 128 We then offer our conclusion in Section 5.

## 129 2 CCPF model

### 130 2.1 The Model

131 Instead of utilizing the original CCPF model that is discrete in space (Bauer et al.  
 132 2000, 2003), we utilize a modified continuum version (Cao et al. 2011, Hua 2009,  
 133 Wang 2010 ). The exchange coefficient in this continuum model differs from that  
 134 of the original CCPF model by a factor of the length of a typical conduit segment.  
 135 A heuristic derivation of this continuum model from the original CCPF model, as  
 136 well as possible pitfalls of this continuum model in three dimension and reasonable  
 137 fixes, are available in the literature (Wang 2010). We will focus on the two spatial  
 138 dimension case for simplicity in this work.

#### 139 2.1.1 The CCPF model

140 Under the simplifying assumptions on the geometry of the domain and the homo-  
 141 geneity and isotropy of the porous media, the continuum version of coupled contin-  
 142 uum pipe flow model for laminar flow takes the form ( Cao et al 2011; Hua 2009;  
 143 Shoemaker et al 2008, Wang 2010)

$$\begin{cases} -\mathcal{K}\Delta\phi_m = -\alpha_{ex}(\phi_m - \phi_c)\delta_{y=0} + S_m & \text{in } \Omega_m \\ -D\frac{\partial^2\phi_c}{\partial x^2} = \alpha_{ex}(\phi_m(0) - \phi_c) + S_c & \text{in } \Omega_c \end{cases} \quad (1)$$

144 where  $\Omega_m = (0, L) \times (0, H_m) \cup (0, L) \times (-H_m, 0)$  and  $\Omega_c = (0, L) \times \{y = 0\}$  are the  
 145 regions for the matrix and conduit respectively,  $\mathbb{K} = \mathcal{K}\mathbb{I}$  is the hydraulic conductivity

146 tensor (where  $\mathcal{K}$  is taken to be a constant under the homogeneous isotropic media  
 147 assumption),  $\phi_m$  is the hydraulic head in the porous matrix,  $\phi_c$  is the hydraulic  
 148 head in the conduit,  $\alpha_{ex}$  is the fluid exchange coefficient between the matrix and  
 149 the conduit (the key parameter to be calibrated),  $\delta_{y=0}$  is the Dirac delta function  
 150 concentrated on the conduit  $y = 0$ , and  $S_m$  and  $S_c$  are source terms (which will be  
 151 set to zero in this study).  $D = \frac{d^3 g}{12\nu}$ , where  $d$  is the diameter (or the width in two  
 152 dimensional case) of the conduit,  $g$  is the Earth's gravitational acceleration,  $\nu$  is the  
 153 kinematic viscosity of water, and  $\phi_m(0)$  represents the restriction of  $\phi_m$  along the  
 154 line  $y = 0$ .

155 The first equation is a consequence of Darcy's equation in the matrix where the  
 156 second term in the equation models fluid exchange between the conduit and matrix  
 157 via Barenblatt type approach. The second equation is a consequence of conservation  
 158 of mass in the conduit where the flow in the conduit is modeled via pipe flow model,  
 159 and the second term in the equation models fluid exchange.

### 160 2.1.2 The boundary conditions

161 As we mentioned earlier in the introduction, we will postulate the following Neumann  
 162 boundary condition which is equivalent to specifying the flux at the boundary :

$$\left\{ \begin{array}{l} \frac{\partial \phi_m}{\partial x} \Big|_{x=0} = f_{ml}, \quad \frac{\partial \phi_m}{\partial x} \Big|_{x=L} = f_{mr}, \\ \frac{\partial \phi_c}{\partial x} \Big|_{x=0} = f_{cl}, \quad \frac{\partial \phi_c}{\partial x} \Big|_{x=L} = f_{cr}, \\ \frac{\partial \phi_m}{\partial y} \Big|_{y=\pm H_m} = 0. \end{array} \right. \quad (2)$$

163 Due to the incompressibility of the model, we must have the following *compatibil-*  
 164 *ity* condition satisfied on the boundary conditions (equivalent to mass conservation):

$$2\mathcal{K}H_m(f_{mr} - f_{ml}) + D(f_{cr} - f_{cl}) = 0. \quad (3)$$

165 It is easy to observe that the case with prescribed head can be investigated in

166 a similar fashion. However, we will not focus on this part since the Stokes-Darcy  
 167 system does not seem to enjoy straightforward Fourier expansion in the horizontal  
 168 direction under prescribed pressure head boundary condition.

## 169 2.2 Solution to the CCPF model

### 170 2.2.1 Solution strategy

171 Due to the prescribed constant Neumann boundary condition, we can now define  
 172 the following two new unknowns

$$\frac{\partial \tilde{\phi}_m}{\partial x}(x, y) = \frac{\partial \phi_m}{\partial x}(x, y) - (f_{ml} + \frac{x}{L}(f_{mr} - f_{ml})), \quad (4)$$

$$\tilde{\phi}'_c(x) = \phi'_c(x) - (f_{cl} + \frac{x}{L}(f_{cr} - f_{cl})). \quad (5)$$

173 It is easy to see that  $\frac{\partial \tilde{\phi}_m}{\partial x}(0, y) = \frac{\partial \tilde{\phi}_m}{\partial x}(L, y) = 0$  and  $\tilde{\phi}'_c(0) = \tilde{\phi}'_c(L) = 0$ , giving  
 174 us homogeneous Neumann boundary conditions. Therefore we can employ Fourier  
 175 cosine expansion in the  $x$  variable to reduce the CCPF model Eq. (1) into an infinite  
 176 system of decoupled ODEs for the Fourier coefficients that we can solve mode by  
 177 mode.

### 178 2.2.2 The CCPF solution formula

179 Solving the infinite decoupled ODEs for the Fourier coefficients and converting the  
 180 Fourier mode solution for the translated unknowns back into our original variables,  
 181 we deduce the following solution formula to the CCPF model:

$$\begin{aligned}
\phi_m(x, y) = & f_{ml}x + \frac{1}{2L}(f_{mr} - f_{ml})(x^2 - y^2) + B \\
& + \begin{cases} \frac{H_m}{L}(f_{mr} - f_{ml})y + \sum_{k=1}^{\infty} \mathcal{C}_k (e^{\frac{k\pi y}{L}} + e^{\frac{k\pi}{L}(2H_m - y)}) \cos\left(\frac{k\pi x}{L}\right), & y \in (0, H_m) \\ -\frac{H_m}{L}(f_{mr} - f_{ml})y + \sum_{k=1}^{\infty} \mathcal{C}_k (e^{\frac{k\pi}{L}(2H_m + y)} + e^{-\frac{k\pi y}{L}}) \cos\left(\frac{k\pi x}{L}\right), & y \in (-H_m, 0) \end{cases}
\end{aligned} \tag{6}$$

$$\begin{aligned}
\phi_c(x) = & f_{cl}x + \frac{1}{L}(f_{cr} - f_{cl}) \left( \frac{x^2}{2} + \frac{D}{\alpha_{ex}} \right) + B + \frac{L}{6}(f_{mr} + 2f_{ml} - f_{cr} - 2f_{cl}) \\
& + \sum_{k=1}^{\infty} \frac{\alpha_{ex} [\mathcal{C}_k (1 + e^{\frac{2k\pi H_m}{L}}) - \hat{S}_k]}{\alpha_{ex} + \frac{k^2\pi^2}{L^2} D} \cos\left(\frac{k\pi x}{L}\right)
\end{aligned} \tag{7}$$

182 where B is an arbitrary constant (head is only determined up to a constant), and  
183 the coefficients are given by

$$\mathcal{C}_k = \frac{c_{0,k}L}{2k\pi(1 - e^{\frac{2k\pi H_m}{L}})}, \tag{8}$$

184 with

$$c_{0,k} = \frac{2\alpha_{ex} D \frac{k^2\pi^2}{L^2} \hat{S}_k (1 - e^{\frac{2k\pi H_m}{L}})}{\alpha_{ex} D \frac{k\pi}{L} (1 + e^{\frac{2k\pi H_m}{L}}) - 2\mathcal{K} (1 - e^{\frac{2k\pi H_m}{L}}) (\alpha_{ex} + D \frac{k^2\pi^2}{L^2})} \tag{9}$$

185 and

$$\hat{S}_k = \frac{2L}{(k\pi)^2} [(f_{ml} - f_{cl}) - (-1)^k (f_{mr} - f_{cr})]. \tag{10}$$

## 186 **3 The coupled Stokes-Darcy system**

### 187 3.1 The Stokes-Darcy model

#### 188 3.1.1 The model

The coupled Stokes-Darcy model for laminar flow in the karst aquifer under consideration takes the form (Beavers and Joseph 1967, Cao et al 2010b, Discacciati et al. 2002, Layton et al. 2003, Nield 1977 )

$$\left\{ \begin{array}{l} \frac{\nu n}{\Pi} \vec{u}_m + n \nabla p_m = -ng\vec{j}, \quad \nabla \cdot \vec{u}_m = 0, \quad \text{in } \Omega_m, \\ -2\nu \nabla \cdot \mathbb{D}(\vec{u}_c) + \nabla p_c = -g\vec{j}, \quad \nabla \cdot \vec{u}_c = 0, \quad \text{in } \Omega_c, \end{array} \right. \quad (1)$$

189 where  $\vec{j} = (0, 1)^T$  denotes the unit vector in (upward) vertical direction,  $\Omega_m =$   
 190  $(0, L) \times (H_c, H_c + H_m) \cup (0, L) \times (-H_m - H_C, -H_c)$  and  $\Omega_c = (0, L) \times (-H_c, H_c)$  are  
 191 the regions for the matrix and conduit respectively,  $\vec{u}_m$ ,  $\vec{u}_c$ ,  $p_m$  and  $p_c$  are the velocity  
 192 and the kinematic pressure in the matrix and conduit respectively,  $\nu$  denotes the  
 193 kinematic viscosity,  $n$  the porosity,  $\Pi$  the permeability, and  $\mathbb{D}(\vec{u}) = \frac{1}{2}(\nabla \vec{u} + (\nabla \vec{u})^T)$   
 194 the deformation rate tensor.

195 The first equation is the classical Darcy's equation characterizing fluid flow in  
 196 the matrix while the second equation is the standard Stokes equations governing  
 197 the motion of fluid in the conduit. Compared to the CCPF model, the flow in the  
 198 conduit is now modeled via the Stokes equations instead of the simple pipe flow.  
 199 Moreover, the fluid exchange is no longer explicitly included in the equations but  
 200 modeled through interface boundary conditions described in the next subsection  
 201 instead of in an ad-hoc fashion as in the CCPF model.

#### 202 3.1.2 Boundary and interface conditions

203 We need to equip the Stokes-Darcy system Eq. (1) with boundary conditions that are  
 204 compatible with the Neumann boundary condition for the CCPF model Eq. (2). For

205 the pressure in the matrix, we prescribe Neumann boundary condition (equivalent  
 206 to prescribed flux). For the velocity in the conduit, we utilize the stream function  
 207  $\psi$  which is related to the velocity through

$$\vec{u}_c = \left( -\frac{\partial\psi}{\partial y}, \frac{\partial\psi}{\partial x} \right) = \nabla^\perp\psi. \quad (2)$$

208 and we will prescribe the value of the stream function  $\psi$  at the ends of the conduit  
 209 ( $x = 0, L$ ) that are compatible with parabolic profile. Therefore we postulate the  
 210 following boundary conditions.

$$\begin{aligned} \frac{\partial p_m}{\partial x}(x, y)|_{x=0} &= g \cdot f_{ml}, & \frac{\partial p_m}{\partial x}(x, y)|_{x=L} &= g \cdot f_{mr}, \\ \frac{\partial p_m}{\partial y}(x, y)|_{y=\pm(H_m+H_c)} &= -g, \\ \psi|_{x=0} &= c_l \left( \frac{y^3}{3H_c^2} - y \right), & \psi|_{x=L} &= c_r \left( \frac{y^3}{3H_c^2} - y \right). \end{aligned} \quad (3)$$

211 together with the following classical empirical Beavers-Joseph boundary conditions  
 212 (Beavers and Joseph 1967)

$$\begin{aligned} \vec{u}_c \cdot \vec{n}_{mc} &= \vec{u}_m \cdot \vec{n}_{mc}, \\ -\vec{n}_{mc} \cdot (\mathbb{T}(\vec{u}_c, p_c)\vec{n}_{mc}) &= p_m, \\ -\vec{\tau}_{mc} \cdot (\mathbb{T}(\vec{u}_c, p_c)\vec{n}_{mc}) &= \alpha_{BJ} \frac{\nu}{\sqrt{\Pi}} \vec{\tau}_{mc} \cdot (\vec{u}_c - \vec{u}_m), \end{aligned} \quad (4)$$

213 where  $\alpha_{BJ}$  is an empirical constant determined by the geometry and the material  
 214 (will be set to  $\alpha_{BJ} = 1$  for simplicity in this study),  $\vec{n}_{mc}$  is the unit outer normal to  
 215 the matrix at the interface, and  $\vec{\tau}_{mc} = (1, 0)$  is the (positive) unit tangent vector to  
 216 the interface.

217 The boundary conditions on the pressure in porous media in Equation (3) are  
 218 consistent with the boundary condition on the head in the porous media for the  
 219 CCPF model in Equation (2) since

$$h_m = \frac{p_m}{g} + y. \quad (5)$$

220 The prescribed boundary value for the stream-function in Equation (3) implies that  
 221 the horizontal velocity in the conduit enjoys the following parabolic profile

$$u_{c,1}|_{x=0} = v_l(y) := -c_l \left( \frac{y^2}{H_c^2} - 1 \right), \quad u_{c,1}|_{x=r} = v_r(y) := -c_r \left( \frac{y^2}{H_c^2} - 1 \right). \quad (6)$$

222 The constants in the parabolic profiles for flow in the conduit must be taken in the  
 223 following manner so that they are consistent with the specified discharge (flux) for  
 224 the CCPF model Eq. (2)

$$f_{cr} = \frac{-4c_r H_c}{3D}, \quad f_{cl} = \frac{-4c_l H_c}{3D}. \quad (7)$$

225 The mass conservation then dictates

$$f_{mr} - f_{ml} = \frac{-2(c_l - c_r)H_c}{3\mathcal{K}H_m} \quad (8)$$

226 which is equivalent to Equation (3).

227 It is worthwhile to point out that the case with prescribed head can be considered  
 228 as well in principle. However the Fourier methodology may not be applicable. For  
 229 instance, fixed head implies Fourier sine expansion (after appropriate translation)  
 230 for the pressure in the conduit while parabolic profile also suggests Fourier sine  
 231 expansion (after appropriate translation) for the horizontal velocity in the conduit,  
 232 and these two sine expansions are not consistent with the Stokes equations (1).

233 It should be noted that the horizontal ( $x$ ) derivative of the stream function should  
 234 be specified at the ends of the conduit ( $x = 0, L$ ) as well in order to specify the  
 235 whole velocity. This is implicitly done here by the incompressible condition and the  
 236 assumption that the translated stream-function (10) enjoys sine expansion in the  $x$   
 237 direction in both  $L^2$  and  $H^1$  space (hence the translated vertical velocity satisfies  
 238 homogeneous Neumann boundary at condition at the ends of the conduit).

## 239 3.2 Solution to the Stokes-Darcy system

### 240 3.2.1 Solution strategy

241 For the Darcy part, we use the pressure  $p_m$  as the main (prognostic) variable which  
 242 satisfies the Laplace equation. Introducing the following translated new unknown

$$\tilde{p}_m = p_m - g \left[ x \cdot f_{ml} + \frac{x^2}{2L}(f_{mr} - f_{ml}) \right], \quad (9)$$

243 which is equipped with homogeneous Neumann boundary condition  $\frac{\partial \tilde{p}_m}{\partial x}(0, y) = 0 =$   
 244  $\frac{\partial \tilde{p}_m}{\partial x}(L, y)$ . Therefore we could employ Fourier cosine expansion in the  $x$  variable for  
 245  $\tilde{p}_m$ .

246 As for the Stokes part, we work with the stream-function  $\psi$  which satisfies the  
 247 bi-harmonic equation  $\Delta^2 \psi = 0$ . In order to homogenize the boundary conditions at  
 248 the lateral ends, we introduce the following translated stream-function

$$\tilde{\psi}(x, y) = \psi(x, y) + \int_0^y \left[ v_l(s) + \frac{x}{L}(v_r(s) - v_l(s)) \right] ds. \quad (10)$$

249 This translated stream-function is zero (homogeneous Dirichlet boundary condition)  
 250 at the lateral ends ( $x = 0, L$ ). Hence, the translated velocity  $\tilde{u}_c = \nabla^\perp \tilde{\psi}$  satisfies  
 251 the homogenous Dirichlet boundary condition for the horizontal velocity  $\tilde{u}_{c,1}$ , and  
 252 homogeneous Neumann boundary condition for the translated vertical velocity  $\tilde{u}_{c,2}$   
 253 at the lateral ends. Therefore we could employ Fourier sine expansion in  $x$  for the  
 254 translated horizontal velocity and the stream function, and Fourier cosine expansion  
 255 in  $x$  for the translated vertical velocity and pressure in the conduit.

### 256 3.2.2 Solution formula for the Stokes-Darcy model

257 Solving the resulting infinitely many decoupled constant coefficient ODEs for the  
 258 Fourier coefficients and revert back to the original variable, we deduce the following  
 259 solution formula for the Stokes-Darcy system Eq. (1) together with the boundary  
 260 conditions Eq. (3) and interface conditions Eq. (4).

The head in the matrix is given by

$$\begin{aligned}
 h_m(x, y) = & f_{ml}x + \frac{1}{2L}(f_{mr} - f_{ml})(x^2 - y^2) + B' \\
 & + \begin{cases} \frac{H_m + H_c}{L}(f_{mr} - f_{ml})y + \frac{1}{g} \sum_{k=1}^{\infty} (C_5 e^{\frac{k\pi y}{L}} + C_6 e^{-\frac{k\pi y}{L}}) \cos\left(\frac{k\pi x}{L}\right), & y > H_c \\ -\frac{H_m + H_c}{L}(f_{mr} - f_{ml})y + \frac{1}{g} \sum_{k=1}^{\infty} (C_7 e^{\frac{k\pi y}{L}} + C_8 e^{-\frac{k\pi y}{L}}) \cos\left(\frac{k\pi x}{L}\right), & y < -H_c, \end{cases}
 \end{aligned} \tag{11}$$

and the velocity in the conduit is given by

$$\begin{aligned}
 u_{c,1}(x, y) = & v_l(y) + \frac{x}{L}(v_r(y) - v_l(y)) + \sum_{k=1}^{\infty} \left[ -\frac{k\pi}{L}C_1 e^{\frac{k\pi y}{L}} + \frac{k\pi}{L}C_2 e^{-\frac{k\pi y}{L}} \right. \\
 & \left. - \left(1 + \frac{k\pi y}{L}\right) C_3 e^{\frac{k\pi y}{L}} - \left(1 - \frac{k\pi y}{L}\right) C_4 e^{-\frac{k\pi y}{L}} \right] \sin\left(\frac{k\pi x}{L}\right) \\
 u_{c,2}(x, y) = & -\frac{1}{L} \int_0^y (v_r(s) - v_l(s)) ds + \sum_{k=1}^{\infty} \left[ \frac{k\pi}{L}C_1 e^{\frac{k\pi y}{L}} + \frac{k\pi}{L}C_2 e^{-\frac{k\pi y}{L}} \right. \\
 & \left. + \frac{k\pi}{L}C_3 y e^{\frac{k\pi y}{L}} + \frac{k\pi}{L}C_4 y e^{-\frac{k\pi y}{L}} \right] \cos\left(\frac{k\pi x}{L}\right)
 \end{aligned} \tag{12}$$

where the coefficients  $C_1$ – $C_8$  are determined via solving the following systems of

linear algebraic equations:

$$e^{\frac{k\pi(H_m+H_c)}{L}} C_5 - e^{-\frac{k\pi(H_m+H_c)}{L}} C_6 = 0 \tag{C1}$$

$$e^{-\frac{k\pi(H_m+H_c)}{L}} C_7 - e^{\frac{k\pi(H_m+H_c)}{L}} C_8 = 0 \tag{C2}$$

$$e^{\frac{k\pi H_c}{L}} C_1 + e^{-\frac{k\pi H_c}{L}} C_2 + H_c \left( e^{\frac{k\pi H_c}{L}} C_3 + e^{-\frac{k\pi H_c}{L}} C_4 \right) + \frac{\Pi}{\nu} \left( e^{\frac{k\pi H_c}{L}} C_5 - e^{-\frac{k\pi H_c}{L}} C_6 \right) = 0 \tag{C3}$$

$$\begin{aligned}
2\nu \left(\frac{k\pi}{L}\right)^2 & \left[ -C_1 e^{\frac{k\pi H_c}{L}} + C_2 e^{-\frac{k\pi H_c}{L}} - H_c \left( C_3 e^{\frac{k\pi H_c}{L}} - C_4 e^{-\frac{k\pi H_c}{L}} \right) \right] - C_5 e^{\frac{k\pi H_c}{L}} - C_6 e^{-\frac{k\pi H_c}{L}} \\
& = \widehat{P}_{m,k}(H_c) - \frac{2\nu k\pi}{L} \widehat{F}_{c,1,k}(H_c) + \frac{L\nu}{k\pi} \widehat{F}_{c,1,k}''(H_c) \quad (\text{C4})
\end{aligned}$$

$$\begin{aligned}
& \left( 2 \left(\frac{k\pi}{L}\right)^2 + \frac{k\pi\alpha_{BJ}}{L\sqrt{\Pi}} \right) e^{\frac{k\pi H_c}{L}} C_1 + \left( 2 \left(\frac{k\pi}{L}\right)^2 - \frac{k\pi\alpha_{BJ}}{L\sqrt{\Pi}} \right) e^{-\frac{k\pi H_c}{L}} C_2 \\
& + \left( 2\frac{k\pi}{L} + \frac{\alpha_{BJ}}{\sqrt{\Pi}} \right) \left( 1 + \frac{k\pi H_c}{L} \right) e^{\frac{k\pi H_c}{L}} C_3 + \left( -2\frac{k\pi}{L} + \frac{\alpha_{BJ}}{\sqrt{\Pi}} \right) \left( 1 - \frac{k\pi H_c}{L} \right) e^{-\frac{k\pi H_c}{L}} C_4 \\
& + \frac{k\pi\alpha_{BJ}\sqrt{\Pi}}{L\nu} \left( e^{\frac{k\pi H_c}{L}} C_5 + e^{-\frac{k\pi H_c}{L}} C_6 \right) = \widehat{F}'_{c,1,k}(H_c) + \frac{\alpha_{BJ}}{\sqrt{\Pi}} \left( \widehat{F}_{c,1,k}(H_c) + \frac{\Pi}{\nu} \widehat{F}_{m,1,k}(H_c) \right) \quad (\text{C5})
\end{aligned}$$

$$e^{-\frac{k\pi H_c}{L}} C_1 + e^{\frac{k\pi H_c}{L}} C_2 - H_c \left( e^{-\frac{k\pi H_c}{L}} C_3 + e^{\frac{k\pi H_c}{L}} C_4 \right) + \frac{\Pi}{\nu} \left( e^{-\frac{k\pi H_c}{L}} C_7 - e^{\frac{k\pi H_c}{L}} C_8 \right) = 0 \quad (\text{C6})$$

$$\begin{aligned}
2\nu \left(\frac{k\pi}{L}\right)^2 & \left[ -e^{-\frac{k\pi H_c}{L}} C_1 + e^{\frac{k\pi H_c}{L}} C_2 + H_c \left( e^{-\frac{k\pi H_c}{L}} C_3 - e^{\frac{k\pi H_c}{L}} C_4 \right) \right] - e^{-\frac{k\pi H_c}{L}} C_7 - e^{\frac{k\pi H_c}{L}} C_8 \\
& = \widehat{P}_{m,k}(-H_c) - \frac{2\nu k\pi}{L} \widehat{F}_{c,1,k}(-H_c) + \frac{L\nu}{k\pi} \widehat{F}_{c,1,k}''(-H_c) \quad (\text{C7})
\end{aligned}$$

$$\begin{aligned}
& \left( -2 \left( \frac{k\pi}{L} \right)^2 + \frac{k\pi\alpha_{BJ\nu}}{L\sqrt{\Pi}} \right) e^{-\frac{k\pi H_c}{L}} C_1 - \left( 2 \left( \frac{k\pi}{L} \right)^2 + \frac{k\pi\alpha_{BJ\nu}}{L\sqrt{\Pi}} \right) e^{\frac{k\pi H_c}{L}} C_2 \\
& + \left( -2 \frac{k\pi}{L} + \frac{\alpha_{BJ\nu}}{\sqrt{\Pi}} \right) \left( 1 - \frac{k\pi H_c}{L} \right) e^{-\frac{k\pi H_c}{L}} C_3 + \left( 2 \frac{k\pi}{L} + \frac{\alpha_{BJ\nu}}{\sqrt{\Pi}} \right) \left( 1 + \frac{k\pi H_c}{L} \right) e^{\frac{k\pi H_c}{L}} C_4 \\
& + \frac{k\pi\alpha_{BJ}\sqrt{\Pi}}{L} \left( e^{-\frac{k\pi H_c}{L}} C_7 + e^{\frac{k\pi H_c}{L}} C_8 \right) = -\widehat{F}'_{c,1,k}(-H_c) + \frac{\alpha_{BJ\nu}}{\sqrt{\Pi}} \left( \widehat{F}_{c,1,k}(-H_c) + \frac{\Pi}{\nu} \widehat{F}_{m,1,k}(-H_c) \right)
\end{aligned} \tag{C8}$$

265 and

$$\begin{aligned}
\widehat{F}_{m,1,k}(y) &= \frac{2g}{k\pi} [f_{ml} - (-1)^k f_{mr}] \quad \text{for } k \neq 0, \\
\widehat{F}_{m,2,0}(y) &= g,
\end{aligned} \tag{13}$$

$$\begin{aligned}
\widehat{F}_{c,1,k}(y) &= \frac{2}{k\pi} [(1 - (-1)^k)v_l(y) - (-1)^k(v_r(y) - v_l(y))], \\
\widehat{F}_{c,2,0}(y) &= -\frac{1}{L} \int_0^y (v_r(s) - v_l(s)) ds.
\end{aligned} \tag{14}$$

266 The constant  $B'$  should be set in the following way so that head difference be-  
267 tween the Stokes-Darcy system and the CCPF model can be minimized:

$$B' = B - \frac{H_c}{L} (f_{mr} - f_{ml}) \left( H_m + \frac{H_c}{2} \right). \tag{15}$$

268 It is observed that the above linear algebraic system for the coefficients  $C_1 - C_8$   
269 could be very stiff for large  $k$ . However, this stiffness is much easier to handle than  
270 the stiffness matrix associated with direct numerical discretization.

## 271 4 Calibration results

272 Here we calibrate the fluid exchange coefficient  $\alpha_{ex}$  by matching the solution to  
273 the CCPF model to that of the Stokes-Darcy model based on the solution formulas

274 presented in the previous two sections. We used 1000 modes in the horizontal  
 275 direction (truncation wave number in  $k$ ) for our numerical calculation. The 1000  
 276 modes contains more than 99% of the energy of all solutions.

## 277 4.1 Criteria

278 There are several criteria that can be used to calibrate the (near) optimal choice  
 279 of the fluid exchange coefficient  $\alpha_{ex}$  as we mentioned earlier in the introduction. The  
 280 criteria (in the  $L^2$  norm) that can be used are

- 281 1. head on the interface, i.e.,  $\sqrt{\int_0^L |\phi_m(x, 0) - h_m(x, H_c)|^2 dx}$ ;
- 282 2. the normal velocity on the interface which is equivalent to fluid exchange rate  
 283 between the conduit and the matrix, i.e.,  $\mathcal{K} \sqrt{\int_0^L \left( \frac{\partial \phi_m(x, y)}{\partial y} \Big|_{y=0} - \frac{\partial h_m(x, y)}{\partial y} \Big|_{y=H_c} \right)^2 dx}$ ;
- 284 3. the head in the matrix, i.e.,  $\sqrt{\int_0^{H_m} \int_0^L |\phi_m(x, y) - h_m(x, y + H_c)|^2 dx dy}$ ;
- 285 4. the velocity in the matrix, i.e.,  $\mathcal{K} \sqrt{\int_0^{H_m} \int_0^L |\nabla \phi_m(x, y) - \nabla h_m(x, y + H_c)|^2 dx dy}$ ;
- 286 and
- 287 5. the discharge in the conduit, i.e.,  $\sqrt{\int_0^L \left| -D\phi'_c(x) - \int_{-H_c}^{H_c} u_{c,1}(x, y) dy \right|^2 dx}$ .

288 As we will see below that the optimal fluid exchange coefficient depends on the  
 289 choice of the matching criterion used. Fortunately, it seems that there is some kind  
 290 of universality in the sense that an order one choice for the exchange coefficient  
 291 works for all criteria reasonably well.

## 292 4.2 Wakulla Spring Parameters

293 We have performed numerical experiments on a set of data corresponding the Wakulla  
 294 Spring in Florida. Additional numerical experiments on a data set corresponding to  
 295 a laboratory set-up investigated earlier (Faulkner et al. 2009) have been performed  
 296 with very much the same result and hence will not be reported here for the sake of  
 297 brevity.

298 We chose parameters for our numerical experiments based on a real life example:  
 299 Wakulla Spring. Wakulla Spring, located near Tallahassee, Florida, is one of the  
 300 largest and deepest freshwater springs in the world. The parameters (together with  
 301 their units) used in the numerics for a flood season are summarized below: Horizontal  
 302 aquifer length (m)  $L = 32000$ ; Height of the matrix (m)  $H_m = 100$ ; Half the height  
 303 of the conduit (m)  $H_c = 2$ ; Conduit inflow velocity at  $y = 0$  (m/s)  $c_l = 0.33H_c^2$ ;  
 304 Conduit outflow velocity at  $y = 0$  (m/s)  $c_r = 0.32H_c^2$  ( $c_l > c_r$  and hence a flood  
 305 season); Gravity acceleration constant (m/s<sup>2</sup>)  $g = 9.8$ ; Kinematic viscosity for water  
 306 (m<sup>2</sup>/s)  $\nu = 10^{-6}$ ; Height of conduit (m)  $d = 2H_c$  (this implies that the constant  $D$   
 307 in the CCPF model is given by:  $D = \frac{gd^3}{12\nu}$  and the unit is (m<sup>2</sup>/s)); Permeability (m<sup>2</sup>)  
 308  $\Pi = \frac{350 \times 10^{-6}}{3600 \times 24g}$ ; Hydraulic Conductivity (m/s)  $\mathcal{K} = \frac{\Pi g}{\nu}$ ; Normal derivative of head in  
 309 the matrix on the left lateral boundary (m/s)  $f_{ml} = -5 \times 10^{-4} \mathcal{K}^{-1}$ ; Normal derivative  
 310 of head in the conduit on the right end (m/s)  $f_{cr} = \frac{-4c_r H_c}{3D}$ ; Normal derivative of head  
 311 in the conduit on the left end (m/s)  $f_{cl} = \frac{-4c_l H_c}{3D}$ ; Normal derivative of head in the  
 312 matrix on the right lateral boundary (m/s)  $f_{mr} = \frac{-2(c_l - c_r)H_c}{3\mathcal{K}H_m} + f_{ml}$ ; CCPF constant  
 313 (m)  $B = -\frac{L}{3}f_{ml} - \frac{L}{6}f_{mr}$  (this is chosen so that the relative error in head can be  
 314 big); Stokes-Darcy constant (m)  $B' = B - \frac{H_c}{L}(f_{mr} - f_{ml})(H_m + \frac{H_c}{2})$ ; Beavers-Joseph  
 315 constant (m)  $\alpha_{BJ} = 1$ .

### 316 4.3 Numerical results

317 The results show the relative error of the root-mean-square ( $L^2$ -norm) of the differ-  
 318 ence of the solutions derived via the two models, instead of the  $L^2$ -norm itself. The  
 319 relative error is computed assuming that the Stokes-Darcy model is the true one.  
 320 These results are computed only up to the 1000<sup>th</sup> Fourier mode for the Wakulla  
 321 Springs data. These 1000 Fourier modes contain more than 99% of the energy  
 322 ( $L^2$ -norm) of all solutions involved.

323 We first tested the conventional wisdom by setting the exchange coefficient  $\alpha_{ex}$   
 324 to be exactly the hydraulic conductivity  $\mathcal{K}$  (Bauer et al. 2000, 2003, Shoemaker

325 et al. 2008). The relative error in terms of head difference on the interface is an  
 326 unacceptable 5000% although the relative error in other measures are much less  
 327 (4.2% in terms of the normal velocity on the interface, 4.7% in terms of the head  
 328 difference in the porous media, and 0.6% in terms of the discharge in the conduit).  
 329 Moreover, there exists high sensitivity on  $\alpha_{ex}$  in this regime of the parameter as  
 330 observed earlier in the literature (Bauer et al. 2000, 2003; Birk et al. 2003; Hua  
 331 2009; Liedl et al. 2003).

332 Next, we tested two extreme cases with  $\alpha_{ex} = 0$  and the limit of  $\alpha_{ex} \rightarrow \infty$ . In  
 333 both cases we discovered that the relative error is nonzero which gives us confidence  
 334 that we can focus on intermediate values for  $\alpha_{ex}$ .

335 It is observed that the relative error never vanishes for the cases that we tested  
 336 (see for instance Figure 2). This implies that the CCPF model is never a perfect  
 337 match of the Stokes-Darcy model. We also observed that there may not be a finite  
 338 value of  $\alpha_{ex}$  that minimizes the relative error. (Our numerics with very large wave  
 339 number  $k$  may not be very reliable due to the stiffness of the linear algebraic system  
 340 for the coefficients  $C_1 - C_8$ .) However, our numerics demonstrate that there is a  
 341 threshold value beyond which the relative error is always below 1% for instance.  
 342 This threshold value of the exchange coefficient will be viewed as near optimal  
 343 choice. The solid curves in Figure 1 describe relative error as a function of  $\alpha_{ex}$   
 344 based on either comparing the discharge in the conduit (bottom right panel), or  
 345 the normal velocity at the interface (top left panel), or head in the matrix (top  
 346 middle panel), or velocity in the matrix, (bottom left), or head at the interface (top  
 347 right). The dotted horizontal line is the line with 1% relative error. Our numerics  
 348 indicate that the relative error will be below the threshold value of 1% provided that  
 349  $\alpha_{ex} \geq 22$  for the case of comparing head on the interface, the normal velocity on  
 350 the interface criterion requires  $\alpha_{ex} \geq 0.02$ , the head in the porous media criterion  
 351 requires  $\alpha_{ex} \geq 0.02$ , the velocity in the matrix criterion requires  $\alpha_{ex} \geq 0.03$ , and the  
 352 discharge in the conduit criterion leads to the constraint  $\alpha_{ex} \geq 3.0 \times 10^{-7}$  with the

353 same threshold level of relative error. Table 1 lists the threshold values of  $\alpha_{ex}$  with  
 354 difference threshold levels of relative error using various criterions.

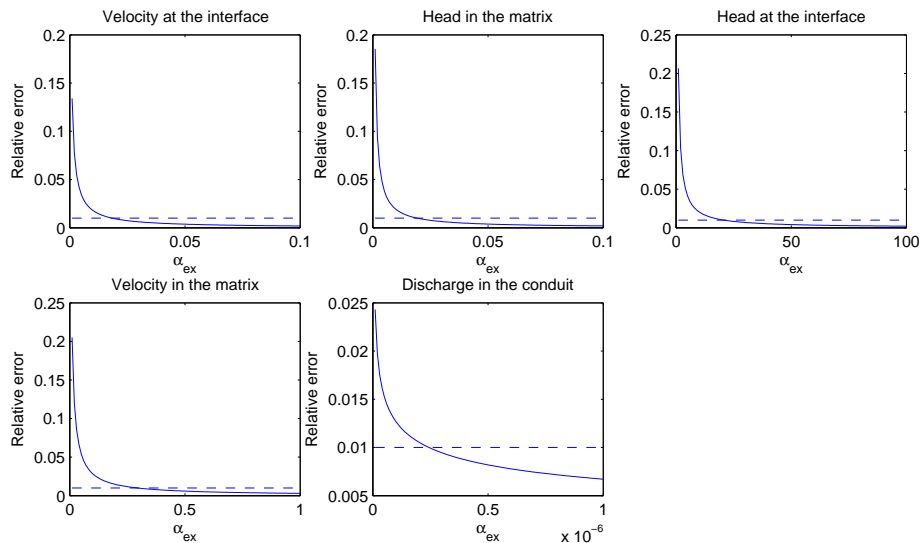


Figure 1: Graphs of the relative errors in the  $L^2$ -norm under different criterions. Each panel shows the critical  $\alpha_{ex}$  value needed to ensure the relative error to be less than or equal to 1%.

355 With the uncertainty concerning the geometry as well as the geological paramete-  
 356 ters associated with the model in mind, we naturally inquire if the numerical results  
 357 that we obtained on the (near) optimal choice of fluid exchange coefficient  $\alpha_{ex}$  are  
 358 robust under perturbation in the geometry and/or geological parameters. Figure 2  
 359 shows the relative error when using normal velocity at the interface as our criterion,  
 360 given different values of several parameters (top left panel: flux in the conduit; top  
 361 right panel: conduit radius; middle left panel: half conduit height; middle right  
 362 panel: permeability; bottom: viscosity). We can observe that an order one choice  
 363 of  $\alpha_{ex}$  will guarantee that the relative error is at most 1%. Figure 3 describes the  
 364 dependence of the threshold value of  $\alpha_{ex}$  corresponding to the 1% relative error and  
 365 variation of parameters (top left panel: flux in the conduit; top right panel: con-  
 366 duit radius; middle left panel: half matrix height; middle right panel: permeability;  
 367 bottom panel: viscosity ) using normal velocity at the interface as criterion.

368 Extensive numerical tests covering a drought season for the Wakulla Springs

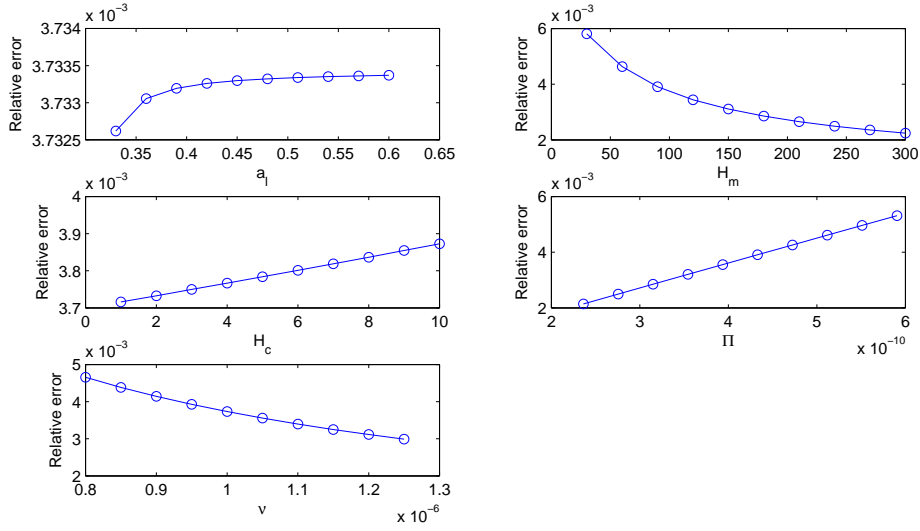


Figure 2: Graphs of the relative error using the optimal  $\alpha_{ex}$  and varying other parameters.

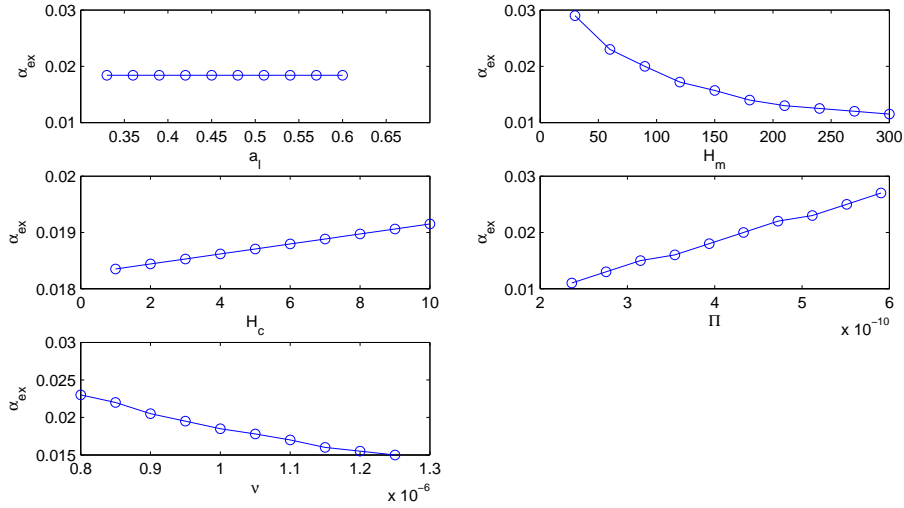


Figure 3: Graphs of the optimal  $\alpha_{ex}$  based on the variation of other parameters. Using this range of  $\alpha_{ex}$ , the relative error will remain under 1%.

369 set-up, flood and drought season for a lab set-up (Faulkner et al. 2009), as well as  
 370 numerous sensitivity tests including sensitivity on the truncation wave number and  
 371 the Beavers-Joseph coefficient (Beavers and Joseph 1967) within the Stokes-Darcy  
 372 model have been conducted. All the numerical results are consistent with the results  
 373 presented here.

## 374 5 Conclusion

375 We have conducted extensive numerical experiments on calibrating the optimal fluid  
 376 exchange coefficient in the CCPF model Eq. (1) assuming the Stokes-Darcy system  
 377 Eq. (1) as the “true model”. Our numerics demonstrate that

- 378 1. The CCPF model is never a perfect match of the Stokes-Darcy model no  
 379 matter how we choose the exchange coefficient  $\alpha_{ex}$ .
- 380 2. The conventional wisdom of setting  $\alpha_{ex}$  to be of the order of the hydraulic  
 381 conductivity may lead to large (up to 5000%) relative error depending on the  
 382 criteria used. Moreover, there exists high sensitivity in this regime of the  
 383 exchange coefficient.
- 384 3. It seems that there exists a natural and universal choice for the fluid exchange  
 385 coefficient  $\alpha_{ex}$  within the CCPF model Eq. (1) that makes the relative error  
 386 small. Indeed, we can set the  $\alpha_{ex}$  sufficiently large (say  $\alpha_{ex} = 25$ ) and obtain  
 387 an upper bound on the relative error (1%). These results are robust under  
 388 perturbation on parameters as well as in truncation wave numbers in our  
 389 numerics. Therefore, the evidences that we have accumulated strongly suggest  
 390 that the CCPF model is an effective simplified model for laminar flow in karst  
 391 aquifer as long as we choose the fluid exchange coefficient appropriately (at  
 392 least 25).

Table 1: Threshold values of  $\alpha_{ex}$  (i.e. the smallest value that alpha can have) to ensure desired bounds on the listed relative error.

Criterion	5%	1%
Comparing the hydraulic head in the matrix	0.004	0.020
Comparing the hydraulic head at the interface	4.2	22
Comparing the normal velocity at the interface	0.004	0.020
Comparing the total discharge in the conduit	$3.0 \times 10^{-9}$	$3.0 \times 10^{-7}$

## 393 Acknowledgment

394 This work is supported in part by grants from the NSF through DMS0620035 (CMG  
395 grant for MG, BH and XW) and DMS1008852 (XW and CW), a COFRS award from  
396 FSU (XW), and an award from the Chinese Ministry of Education for the Modern  
397 Applied Mathematics 111 project in Fudan University (NC and XW).

## 398 References

- 399 1. Barenblatt G., Zheltov I., Kochina I., 1960. Basic concepts in the theory  
400 of seepage of homogeneous liquids in fissured rocks. *J. Appl. Math. Mech.*  
401 (USSR), 24, 1286–1303.
- 402 2. Bauer S., Liedl R., Sauter M., 2000. Modeling of karst development consider-  
403 ing conduit-matrix exchange flow, Calibration and reliability in groundwater  
404 modeling: coping with uncertainty. *Int Assoc of Hydrol Sci* 265:10–15.
- 405 3. Bauer S., Liedl R., Sauter M., 2003. Modeling of karst aquifer genesis: Influ-  
406 ence of exchange flow. *Water Resour Res.* Doi:10.1029/2003WR002218.
- 407 4. Beavers G., Joseph D. D., 1967. Boundary conditions at a naturally permeable  
408 wall. *J Fluid Mech* 30:197–207.
- 409 5. Birk S., Liedl R., Sauter M., Teutsch G., 2003. Hydraulic boundary conditions  
410 as a controlling factor in karst genesis. *Water Resour. Res.*, 39, 1004.
- 411 6. Cao Y., Gunzburger M., Hua F., Wang X., 2010. Coupled Stokes-Darcy model  
412 with Beavers-Joseph interface boundary condition. *Commun in Math Sci* 8:1–  
413 25.
- 414 7. Cao Y., Gunzburger M., Hua F., Wang X., 2011. Analysis and finite element  
415 approximation of a coupled, continuum pipe-flow/Darcy model for flow in

- 416 porous media with embedded conduits. Numer Methods for Partial Differ  
417 Equ. vol. 27, no.5., 1242-1252.
- 418 8. Chen Y., Bian J., 1988. The media and movement of karst water, in Karst  
419 Hydrogeology and Karst Environment Protection: 21st Congress of the In-  
420 ternational Association of Hydrogeologists, Guilin, China, Int. Assoc. of  
421 Hydrogeologists.
- 422 9. Clemens T., Hückinghaus D., Sauter M., Liedl R., Teutsch G., 1996. A com-  
423 bined continuum and discrete network reactive transport model for the simu-  
424 lation of karst development. IAHS Publ., 237, 309–318.
- 425 10. Dershovitz W., Wallmann P., Kindred S., 1991. Discrete fracture network  
426 modeling for the Stripa site characterization and validation drift in flow pre-  
427 dictions. SKB Stripa Technical Teport TR-91-16, Swed. Nucl. Power and  
428 Waste Manage. Co., Stockholm.
- 429 11. Discacciati M., Miglio E., Quarteroni A., 2002. Mathematical and numerical  
430 models for coupling surface and groundwater flows, *Appl. Num. Math.*, 43,  
431 57–74.
- 432 12. Faulkner J., Hu B., Kish S., Hua F., 2009. Laboratory analog and numerical  
433 study of groundwater flow and solute transport in a karst aquifer with conduit  
434 and matrix domains. *J of Contam Hydrol* 110:34–44.
- 435 13. Ford D., 1998. Perspectives in karst hydrology and cavern genesis. *Bull.*  
436 *Hydrogeol.*, 16, 9–29.
- 437 14. Ford D., Williams P., 1989. *Karst Geomorphology and Hydrology*, Chapman  
438 and Hall, New York.
- 439 15. Harbaugh A., 2005. MODFLOW-2005, the U.S. geological survey modular  
440 ground-water model – The ground-water flow process. U.S. Geol Surv Tech

- 441 and Methods 6:A16.
- 442 16. Hua, F., 2009. Modeling, Analysis and Simulation of Stokes-Darcy System  
443 with Beavers-Joseph Interface Condition: PhD, Florida State University, USA.
- 444 17. Katz B., Catches J., Bullen T., Michel R., 1998. Changes in the isotopic and  
445 chemical composition of ground water resulting from a recharge pulse from a  
446 sinking stream. *J. Hydrol.*; 211, 178–207.
- 447 18. Kincaid T., 2004. Exploring the secrets of Wakulla Springs, open seminar,  
448 Tallahassee, FL.
- 449 19. Kiraly L., 1998. Modeling karst aquifers by the combined discrete channel and  
450 continuum approach. *Bull. Hydrogeol.*, 16, 77–98.
- 451 20. Kuniansky E., 2008. U.S. Geological Survey Karst Interest Group Proceedings,  
452 U.S. Geological Survey Scientific Investigations Report 2008-5023, Bowling  
453 Green, 2008.
- 454 21. Layton W.J., Schieweck W., Yotov I., 2003. Coupling fluid flow with porous  
455 media flow, *SIAM J. Num. Anal.*, **40**, 2195-2218.
- 456 22. Liedl R., Sauter M., Hückinghaus D., Clemens T., Teutsch G., 2003. Simula-  
457 tion of the development of karst aquifers using a coupled continuum pipe flow  
458 model. *Water Resour. Res.*, 39, 1057.
- 459 23. MacQuarrie K., Sudicky E., 1996. On the incorporation of drains into three-  
460 dimensional variably saturated groundwater flow models, *Water Resour. Res.*,  
461 32, 447–482.
- 462 24. Nield D.A., 1977. Onset of convection in a fluid layer overlying a layer of a  
463 porous media. *J. Fluid Mech.*, 81: 513-522.
- 464 25. Saffman P., 1971. On the boundary condition at the interface of a porous  
465 medium, *Stud. in Appl. Math.*, **1**, 77-84.

- 466 26. Sauter M., 1992. Quantification and forecasting of regional groundwater flow  
467 and transport in a karst aquifer (Gal lusquel le, Malm SW Germany), Ph.D.  
468 Thesis, Univ. of Tübingen, Tübinger, Germany.
- 469 27. Shoemaker, W. B., Kuniatsky E.L., Birk S., Bauer S., Swain E.D., 2008.  
470 Documentation of a conduit flow process (CFP) for MODFLOW-2005, U.S.  
471 Geological Survey Techniques and method book 6, Chapter A, Reston, Vir-  
472 ginia.
- 473 28. Taylor C., Greene E., 2001. Quantitative Approaches in Characterizing Karst  
474 Aquifers: U.S. Geological Survey Karst Interest Group Proceedings. Water  
475 Resources Investigations Report, 01-4011, 164–166.
- 476 29. Teutsch G., 1989. Two practical examples from the Swabian Alb, S. Germany,  
477 in Proc. 4th Conference on Solving Groundwater Problems with Models, In-  
478 dianapolis, 1989.
- 479 30. Wang X., 2010. On the coupled continuum pipe flow model (CCPF) for flows  
480 in karst aquifer. Discret and Contin Dyn Syst-Ser B 13:489-501.